HHS Public Access

Author manuscript

Mol Neurobiol. Author manuscript; available in PMC 2023 February 01.

Published in final edited form as:

Mol Neurobiol. 2022 February ; 59(2): 1112–1123. doi:10.1007/s12035-021-02637-x.

Differential regulation of neurite outgrowth and growth cone morphology by 3D fibronectin and fibronectin-collagen extracellular matrices

Archana Sharma, **Jean E. Schwarzbauer**

Department of Molecular Biology, Princeton University, Princeton, NJ 08544, USA

Abstract

The extracellular matrix (ECM) plays a critical role in development, homeostasis, and regeneration of tissue structures and functions. Cell interactions with the ECM are dynamic and cells respond to ECM remodeling by changes in morphology and motility. During nerve regeneration, the ECM facilitates neurite outgrowth and guides axons with target specificity. Decellularized ECMs retain structural, biochemical, and biomechanical cues of native ECM and have the potential to replace damaged matrix to support cell activities during tissue repair. To determine the ECM components that contribute to nerve regeneration, we analyzed neuron-ECM interactions on two types of decellularized ECM. One matrix was composed primarily of fibronectin (FN) fibrils, and the other FN-rich ECM also contained significant numbers of type I collagen (COL I) fibrils. Using primary neurons dissociated from superior cervical ganglion (SCG) explants, we found that neurites were extended on both matrices without a significant difference in average neurite length after 24h. The most distinctive features of neurites on the FN matrix were numerous short actin-filled protrusions and longer branches extending from neurite shafts. Very few protrusions and branches were detected on FN-COL matrix. Growth cone morphologies also differed with mostly filopodial growth cones on FN matrix whereas on FN-COL matrix, equivalent numbers of filopodial and slender growth cones were formed. Our work provides new information about how changes in major components of the ECM during tissue repair modulate neuron and growth cone morphologies and helps to define the contributions of neuron-ECM interactions to nerve development and regeneration.

Keywords

Decellularized ECM; SCG neurons; neurite morphology; growth cone; fibronectin

Correspondence to: Jean Schwarzbauer, Ph: (609) 258-2893, jschwarz@princeton.edu.

Authors' contributions

Both authors contributed to the study conception and design. Material preparation and data collection were performed by AS. Data analysis and manuscript writing was performed by AS and JES. Both authors read and approved the final manuscript.

Ethics approval (for animals)

All animal experiments were conducted according to the guidelines of the NIH Guide for the Care and Use of Laboratory Animals and with approval by Princeton University Institutional Animal Care and Use Committee (IACUC).

Consent for publication

Authors give their consent to publish in Molecular Neurobiology

Conflicts of interest/Competing interests

None

Introduction

Nerve development and regeneration require productive interactions between neurons and their microenvironment. The extracellular matrix (ECM) is a dynamic component of the cellular microenvironment. The organization, composition, and mechanical properties of the ECM are critical determinants of cell and tissue functions [1,2]. ECM features change throughout development and regeneration with the introduction of stage-specific ECM components and the deposition of ECM proteins that support new tissue growth, cell rearrangements, and rebuilding of damaged structures. Throughout these processes, the ubiquitous ECM protein fibronectin (FN) is present and forms a fibrillar network to support cell adhesion, proliferation, and migration [3]. FN also supports the matrix incorporation of other ECM components such as collagens, growth factors, and proteoglycans. Type I collagen (COL I) is particularly relevant to repair processes as it is a major component of scar tissue [4,5]. Thus, the ideal microenvironment for nerve regeneration includes an appropriate ECM in order to facilitate neural cell adhesion and neurite outgrowth and to guide axons and growth cones with target specificity [6,7].

FN provides binding sites for cell surface integrin receptors and cells respond to remodeling of the ECM by changing integrin engagement which causes changes in morphology through cytoskeletal rearrangements and modulation of intracellular signaling. Understanding how cells respond to changes in the ECM is essential for the development of tissue regeneration strategies [8]. To communicate, neuronal connectivity is very important, and neurons connect or interact with other neurons through neurites, branches (nascent neurites) and growth cones [9,10]. Neurites are extended using ECM fibrils as a guide [11,12]. Polymerization of actin filaments forms protrusions and growth cone filopodia and lamellipodia that also depend on cell-ECM interactions [13]. During repair, for example, neuronal growth cones interact with the provisional ECM to penetrate a lesion site and to reconnect with other axons [14,15]. However, the roles of different ECM proteins in regulating the formation of neurites, protrusions, and growth cones are not well understood.

Many studies have probed neural cell adhesion and migration on surfaces coated with purified ECM proteins. These substrates have been instrumental in identifying receptor-ECM interactions, ECM protein functions, and attractive/repulsive signals [16]. In vivo, however, neurons interact with more complex substrates than single proteins. In fact, the cellular microenvironment consists of ECM protein polymers assembled into fibrils and having multiple components, variable compliance and porosity, and multi-dimensionality. Decellularized matrices have been shown to be functionally different from protein-coated surfaces and to possess properties similar to an in vivo pericellular matrix [3,17–19]. These properties make a decellularized matrix a useful tool for investigating neuron activities in a natural environment. In addition, at injury sites, the provisional ECM undergoes significant changes as repair progresses with remodeling of the fibrillar FN-rich matrix deposited at the time of injury and incorporation of additional components, including COL I [4,20]. Understanding how changes throughout healing affect neuron-ECM interactions is critical for promoting tissue regeneration.

To determine the effects of major ECM proteins found at nerve injury sites, we analyzed primary neuron-ECM interactions using decellularized ECMs produced by cells in culture. The main advantages of matrices derived from cultured cells over those from dissected tissues are that ECM components can be identified and are equivalent from one cell culture to the next and that ECM composition can be controlled and modified by specific additions to the culture. Dissociated superior cervical ganglia (SCG) neurons were used to assess the behavior of neurites and growth cones in response to different substrates. We previously showed that SCG neurons extend neurites along the fibrils of a decellularized FN matrix and that they weave through the three-dimensional (3D) architecture of the fibrillar ECM network [11,12]. To mimic the FN matrices, present at different phases of injury repair, NIH 3T3 fibroblasts were grown with or without ascorbate treatment to yield matrices rich in FN fibrils but varying in the level of COL I. We show that neurite extension, formation of protrusions and branches, and changes in growth cone morphology on SCG neurons are promoted by a decellularized FN matrix and neurite responses are different when the FN matrix also contains COL I fibrils. Our results show that a FN matrix acts as a regenerative microenvironment and that this function is modulated by the incorporation of ascorbate-induced proteins such as COL I. These findings suggest that controlling ECM composition is important for developing functional regenerative materials.

Materials and Methods

Dissection of superior cervical ganglia and cell culture

All the animal experiments were conducted according to the guidelines of Princeton University Institutional Animal Care and Use Committee (IACUC). Sprague-Dawley rats (Hilltop Labs Incorporated, Scottsdale, PA, USA) were euthanized and embryos were dissected out. Superior cervical ganglia (SCG) were harvested from the base of the neck of rat embryos (E16.5-E17.5) and could be stored up to one week in Hibernate-E reagent (Gibco, NY, USA). Sympathetic neurons and non-neuronal cells were dissociated from SCGs using 0.25% trypsin (Gibco) [21]. In all experiments, one-quarter of the cells dissociated from a SCG explant were seeded per well of a 24-well dish. SCG neurons were cultured on decellularized matrices in neuronal growth media which consists of Neurobasal medium, 1% B-27 medium supplement, 1% penicillin/streptomycin (all purchased from Gibco) and 100 ng/ml Nerve Growth Factor (NGF) (Gibco). NIH 3T3 cells (ATCC, Manassas, VA, USA) were cultured in Dulbecco’s modified Eagle’s medium (DMEM) (Hyclone, Logan, UT, USA) supplemented with 10% bovine calf serum (BCS) (Hyclone) and 1% antibiotic/antimycotic (Corning, VA, USA). All the other chemicals used in the study were of analytical grade.

Preparation and characterization of decellularized extracellular matrices

Extracellular matrices were prepared from NIH 3T3 cells using a modified decellularization procedure adapted from [17,22]. NIH 3T3 cells were seeded on coverslips at a cell density of ~ 8×10^4 cells/cm^2 or 1.5×10^5 cells/well in 1ml of complete media (DMEM, 10% BCS) and grown for 4 days. To increase production of collagen fibrils, NIH 3T3 cells were treated with 50 μg/ml ascorbate (Sigma, MO, USA) and replenished after 2 days of culture.

Decellularized matrices were prepared using our decellularization protocol [22]. As a last step, 1 ml of 20 U/ml DNase I (NEB, Ipswich, MA) prepared in sterile DNase buffer was added to each well and incubated for 1h at 37°C. This step removes residual nuclear material that can show up as ambient background signal with subsequent DAPI staining. After DNase 1 treatment, wells were washed twice with sterile deionized water to remove debris or salt present in sample and then twice with PBS. Decellularized matrices were stored in 1ml PBS/ well at 4°C and could be stored for 1 month. FN and FN-COL decellularized matrices were solubilized with SDS lysis buffer (4% SDS, 20mM Tris-HCl, pH 8.8, 2mM EDTA and 200mM PMSF). Protein concentrations were determined by BCA assay. Equal amounts of all samples were electrophoresed on a 6% polyacrylamide/SDS gel and silver stained [17]. The presence of FN and COL I were confirmed by immunoblotting by using R184 rabbit anti-FN polyclonal antiserum (1:50,000) against type III (1–6) [23,24]. Type I collagen was detected with anti-collagen type I antibody A1 (Boster Biological Technology, Pleasanton, CA, USA). Blots were developed with SuperSignal West Pico PLUS Chemiluminescent Substrate (ThermoScientific, Waltham, MA).

Immunofluorescence and microscopy

Non-decellularized and decellularized matrices from NIH 3T3 cells were fixed in 3.7% formaldehyde in PBS and then stained with DAPI (1:500, Sigma), rabbit anti-FN antiserum (R184, diluted 1:100) or rabbit anti–collagen I/COLIA1 polyclonal antibody (diluted 1:500, Boster Biological Technology, Pleasanton, CA, USA) followed by Alexa fluor 488 and Alexa fluor 568 goat anti-rabbit IgG (1:600, Invitrogen, Eugene, OR, USA) respectively [24]. SCG neurons were seeded on decellularized FN and FN-COL matrices for the indicated times and then fixed with 3.7% formaldehyde and permeabilized with 1% Triton X-100 in PBS at room temperature for 15 mins. Microtubules were visualized using monoclonal anti-α-tubulin antibody (1:500, Sigma) followed by Alexa fluor 488 goat anti-mouse IgG (1:600, Invitrogen). Actin filaments were stained with rhodamine-phalloidin (1:100, Invitrogen). Coverslips were mounted using ProLong Gold Antifade reagent (Invitrogen). A Nikon Eclipse Ti inverted microscope with Hamamatsu digital camera was used to capture images. Images were analyzed using Nikon NIS Elements and ImageJ software.

Analyses of neurites and growth cones

Fluorescence images were captured at 24h, 48h, and 72h of neuron culture on decellularized matrices. Quantifications of neurite lengths and of numbers of protrusions and branches were performed using neurons stained with rhodamine-phalloidin. To determine the percent of neurons extending neurites at 24h, individual neurons that were clearly separated from neighboring cells, not in clumps, were counted, and neurites were scored as actin-positive membrane projections longer than the diameter of the cell body. Neurite lengths were measured by tracing with the freehand line tool in ImageJ starting at the cell body and ending at the growth cone where the fluorescent signal becomes wider than the neurite due to presence of actin filaments or filopodia. For neurons with multiple neurites, only the longest neurite was measured. Overlapping or intertwined neurites, for which the ends could not be definitely identified, were excluded from measurements.

Actin-filled projections extending from the neurite shaft and at least as long as the width of the neurite shaft (~2 μm) but less than the diameter of the cell body (10–20 μm) were scored as protrusions. Projections near the growth cone where the neurite shaft widens were not counted as protrusions. Projections that were longer than the diameter of the cell body were scored as branches [25]. The total number (n) of neurites scored for projections across three independent experiments was on FN matrix = 212 (24h), 114 (48h) and 108 (72h), and on FN-COL matrix = 199 (24h), 170 (48h) and 115 (72h). In some cases, a branch would have an obvious secondary growth cone. SCG neurons co-stained for microtubules and actin filaments were analyzed by confocal microscopy and identified two types of growth cones, filopodial and slender. Growth cone morphologies and total areas on different matrices were scored using epifluorescence images stained for actin filaments. The total number (n) of growth cones scored across three independent experiments was: on FN matrix = 102 (24h), 139 (48h) and 125 (72h) and FN-COL matrix = 178 (24h), 115 (48h) and 127 (72h). Neurons from three independent SCG isolations were analyzed. Multiple images were taken at random at each time point.

Statistical analyses

All the graphs were made with GraphPad Prism 8 software. Statistical comparisons between samples at different time points were performed using two-tailed unpaired t-test with Welch correction and one-way ANOVA followed by Bonferroni post-test. Data are shown in bar plots (mean ± SEM) and whisker plots (box representing 25^{th} and 75^{th} percentile, middle line indicating the median, and whiskers representing the min and max values). The results were considered statistically significant when $P \leq 0.05$. All data are presented as mean ± standard error of the mean (SEM).

Results

Preparation and characterization of decellularized matrices

Mouse NIH 3T3 fibroblasts assemble a dense FN-rich ECM that supports neural cell adhesion and migration [11,17,22]. These cells were used to generate a fibrillar ECM that was then decellularized. Matrices stained before and after decellularization show that the fibrillar organization of FN is maintained but that nuclear material is completely removed by the decellularization procedure (Fig. 1). The fibrillar network is maintained throughout decellularization as shown by confocal imaging (Supplementary Fig. S1A). FN was the major protein band when solubilized decellularized matrix was analyzed by SDS-PAGE (Supplementary Fig. 1B). To promote the production and fibrillogenesis of COL I in the matrix, the cell growth medium was supplemented with ascorbate, a cofactor for enzymes involved in collagen biosynthesis and processing [26]. FN fibril densities (Fig. 2A) and FN protein in the matrices (Fig. 2B) appear very similar in matrices from NIH 3T3 cell cultures grown with or without ascorbate. In contrast, matrix obtained from cells grown with ascorbate assembled elaborate collagen fibrils compared to matrix from cells without ascorbate where collagen I staining was diffuse across the matrix (Fig. 2A). Mass spectrometry of solubilized decellularized matrix identified FN as the most abundant protein followed by perlecan and types I and III collagens (Supplementary Table 1). Total spectral counts of these proteins were not significantly different with and without

ascorbate treatment. Only those proteins that had more than 10 total spectral counts are shown (Supplementary Table 1). While mass spectrometry did not detect changes in COL I levels with ascorbate, procollagen processing and collagen fibrillogenesis were dramatically affected in the presence of ascorbate (Fig. 2A, C). Procollagen was the predominant band in the matrix sample without ascorbate, while the inclusion of ascorbate promoted processing of procollagen yielding a major mature collagen band at ~140 kDa and lesser procollagen and partially processed bands at ~200 kDa and ~170 kDa, respectively (Fig. 2C). Bands on immunoblots co-migrate with the major bands detected by silver stain (Supplementary Fig. 1B). Because both matrices are rich in FN but differ in collagen fibrils, we will refer to the 3D matrix from cells without ascorbate as a FN matrix and that from cells grown with ascorbate as a FN-collagen (FN-COL) matrix throughout this work.

Neurite outgrowth on FN and FN-COL matrices

Sympathetic neurons extend neurites from SCG explants on decellularized ECM [11]. However, neurites are very dense and non-neuronal cells in explant cultures further complicate analysis of neurite features. To test whether neurite outgrowth is affected by differences in matrix composition, cells were dissociated from SCG explants and neurons were seeded uniformly on decellularized FN and FN-COL matrices. Dissociated SCG neurons adhered to the decellularized ECMs and neurite extension was detectable by staining actin filaments (Supplementary Fig. 2). Neurite length measurements were made at 24h, 48h, and 72h by tracing from the cell body to the neurite tip and representative images of SCG neurons on FN and FN-COL matrices, with and without tracings, are shown in Supplementary Fig. 2. Short neurites were observed at 24h. At 48h and 72h, neurite lengths had increased substantially, and some neurites were intertwined. Only those neurites that could be traced from the cell body to the tip were included in the analysis. At 24h, a higher percentage of neurons had extended neurites on FN matrix (57%) compared to FN-COL matrix (40%) (Fig. 3A) and the average neurite length was slightly longer on FN matrix (Fig. 3B). When neurite lengths on FN and FN-COL matrices were compared across time, no statistical differences between matrices were detected at later time points (Fig. 3B). However, neurite lengths did increase significantly on the same matrix with each 24h period (Table 1). These data show that both decellularized FN and FN-COL matrices support neuron adhesion and neurite extension by SCG neurons.

Differences in protrusions and branches on FN and FN-COL matrices

As neurites are extended, membrane projections form along the neurite shaft. We evaluated the effects of FN and FN-COL matrices on the formation of protrusions and branches by visualizing and scoring actin filament-based projections. Short, thin actin-filled membrane projections were scored as protrusions, while projections longer than the diameter of the neuronal cell body, in some cases, with a secondary growth cone, were scored as branches [9,10]. Examples of typical protrusions or branches along SCG neurite shafts are shown in Fig. 4A. To evaluate the effects of ECM composition on development of these processes, numbers of protrusions and branches per neurite were counted on different decellularized matrices and average numbers were determined at 24h, 48h and 72h (Table 2). On FN matrix, the number of protrusions per neurite was highest at 24h and gradually decreased with time whereas branches per neurite were highest at 72h and had gradually increased

with time (Fig. 4B, C; Supplementary Fig. 3A). On the other hand, on FN-COL matrix, the number of protrusions per neurite was variable and did not yield an increasing or decreasing trend over time (Fig. 4B). The number of branches per neurite increased between 24h and 48h and then stabilized at 72h (Fig. 4C; Supplementary Fig. 3B). Significantly fewer protrusions were observed on FN-COL matrix compared to FN matrix at any given time point (Fig. 4B). Branch numbers were also significantly lower (except 48h) and only reached half the average number compared to FN matrix at 24h and 72h (Fig. 4C).

To illustrate the distributions of protrusions and branches across the neurite population, we plotted the percentage of neurites containing from 0 to 10 projections. On FN matrix, ~10%, 30% and 35% of neurites were devoid of protrusions at 24h, 48h and 72h, respectively (Fig. 5A, black bars). Similarly, neurites with 1 protrusion increased from ~20% at 24h to ~38% by 72h (blue bars). In contrast to the increases in these two categories, the percent of neurites with 2 or 3 protrusions was relatively constant over time (brown and pink bars). Neurites with 4 or more protrusions showed a decrease from ~35% at 24h, to 18% and < 5% at 48h and 72h, respectively. Branches showed the opposite pattern. Greater than 90% had 0 or 1 branch at 24h, which decreased to ~35% at 72h, while neurites with 2, 3, or 4 branches increased from <10% to >50% in the same period (Fig. 5B). These results suggest a correlation between decreases in protrusion numbers and increases in branches.

Projection of multiple protrusions or branches from a single neurite was much less prevalent on FN-COL matrix than on FN matrix. Greater than 80% of neurites had 0 or 1 protrusion at all time points (Fig. 5C). While 7–10% of neurites had 2 protrusions at 24h and 48h, less than 5% of neurites had 2 or more protrusions by 72h. As with neurites on FN matrix, we also observed an increase in the number of branches on FN-COL matrix over time. >90%, 75% and 70% of neurites had only 0 or 1 branch at 24h 48h, and 72h, respectively (Fig. 5D). Over the same period, the percent with 2 branches increased from <10% to > 20%. 3 or more branches was a minor population even at 72h. The low number of protrusions and branches at all time points suggests that the inclusion of COL I, or perhaps other ascorbate-dependent proteins, in the matrix affects the ability of these projections to form.

In general, the number of protrusions and branches per neurite was higher on FN matrix than on FN-COL matrix. Also, the higher number of protrusions/branches per neurite, with neurites that are on average similar in length, results in projections that are closer together on FN versus FN-COL matrix. While protrusion numbers decreased with time, the number of branches on FN matrix increased over the same time period. Overall, these results support the conclusion that FN matrix promotes extension of protrusions along elongating neurites and some of these might develop into branches. When COL I was enriched in the FN matrix, however, fewer protrusions formed suggesting that deposition of collagen molecules may block processes from forming stable interactions with the FN ECM.

Different morphologies of growth cones on decellularized matrices

Neurons interact with the ECM and extend neurites using growth cones [27–29]. To estimate how different decellularized matrices affect growth cone dynamics, we explored growth cone morphologies on decellularized FN and FN-COL matrices. Cultures were co-stained with fluorescent rhodamine-phalloidin to visualize actin filaments in growth cone filopodia

and with anti-tubulin to detect microtubules in the neurite shafts (Fig. 6A). Two main types of growth cone morphology were identified and counted. Filopodial growth cones are fan-shaped and have two or more distinct filopodia (Fig. 6B). Slender growth cones have a long narrow shape and terminate with one or a few small filopodia; actin and tubulin staining overlap in slender growth cones. More filopodial growth cones and fewer slender growth cones were scored on FN matrix (Fig. 6C, D) and filopodial growth cones were about 4 times more abundant than slender growth cones (Supplementary Fig. 4A). On FN-COL matrix, growth cones were found in approximately equal numbers of slender and filopodial morphologies (Fig. 6C, D; Supplementary Fig. 4B). The proportion of each morphology was consistent across all three time points on both matrices (Table 3). The significant differences in proportions of filopodial and slender growth cones suggest that these two matrices differ in the mechanisms by which they promote neurite growth. To test this idea, we quantified growth cone areas. Slender growth cones were equivalent in size on the two matrices (< 30 μm^2). In sharp contrast, filopodial growth cones were 1.5-fold larger on FN matrix than on FN-COL matrix, averaging 69 ± 7 μm^2 (n = 26) compared to 45 ± 5 μm^2 (n = 21) ($P \leq 0.01$), respectively. These measurements demonstrate that not only were there more filopodial growth cones on FN matrix, but they were also larger than on FN-COL matrix. These findings also support our contention that modulation of neurite outgrowth in the presence of ascorbate-induced proteins occurs through a mechanism that limits growth cone size and extent of interactions between neurites and the FN matrix. Decellularized FN matrix acts as a permissive substrate that facilitates formation of filopodial over slender growth cones. Manipulating the FN matrix composition to increase COL I affects growth cone adhesion resulting in an increase in formation of slender growth cones.

Discussion

At sites of injury, the normal nerve microenvironment is replaced by a provisional matrix rich in FN and the repair processes involve non-neuronal cells and ECM proteins such as collagen that contribute to the healing process. To provide an understanding of how neurons respond to the changes in ECM that occur during repair, we compared decellularized matrices consisting primarily of FN fibrils or with a combination of FN and COL I fibrils. A higher percentage of SCG neurons had neurites and the average length was longer on FN matrix compared to FN-COL matrix at 24h indicating that neurite outgrowth was initiated more quickly on a FN substrate, but ultimately neurite lengths were similar on both matrices. Significant differences between matrices were detected for protrusions, branches, and growth cones. More protrusions and branches were extended from the shafts of neurites on FN matrix than on FN-COL matrix. In addition, the majority of growth cones on FN matrix were filopodial in contrast to growth cones on a FN-COL matrix which were equal proportions of filopodial and slender growth cones. Furthermore, filopodial growth cones covered a larger area of the FN matrix, indicating more numerous contacts between neurons and ECM, than filopodial growth cones on a FN-COL matrix. Together our findings show that the composition of the ECM regulates neurite outgrowth and that the extent of contacts between neuron and FN matrix determine the rate at which neurons form filopodia and protrusions and connect with each other during repair.

Up-regulation of FN plays a crucial role in repair of nerve tissue [30] and axons have been shown to extend across lesions filled with FN and COL I [15]. We mimicked these situations by growing cells with and without ascorbate which promotes collagen fibrillogenesis. Neurites were located within the fibrils of decellularized fibrillar matrix in our experiments, confirming the earlier observations from our lab [11,12]. Neurons extended neurites on both matrices but the number of protrusions, branches, and filopodial growth cones was higher on FN matrix. Staining for localization of focal adhesion proteins that associate with FN-binding integrin receptors supports the conclusion that these processes are contacting FN fibrils in the ECM (A. Sharma, unpublished observations). Other ECM components may be involved in modulating neuron-ECM interactions. The heparan sulfate proteoglycan (HSPG) perlecan was the third most abundant protein detected in both FN and FN-COL matrices by mass spectrometry. Perlecan may be contributing to neurite outgrowth since HSPGs have been shown to affect interactions between neurons and the ECM and HSPGs can also function as attractive signals for neurite outgrowth [31,32]. Chondroitin sulfate (CS) PGs, on the other hand, have been shown to impede neurite outgrowth during repair [31,33,34] but the levels in the decellularized matrices used here were very low in our mass spectrometry dataset and therefore not likely to cause the sizeable differences in protrusions, branches, and filopodial growth cones we observed.

Two types of growth cone were identified and differed in size and proportion depending on the ECM [27,29]. The more extensive interactions of filopodial growth cones are associated with a higher incidence of pausing during migration [35]. Pausing behavior in growth cone migration may leave a mark that can then become a future branch site [10,36,37] suggesting a connection between growth cone size and numbers of protrusions/branches on a FN matrix. Furthermore, it has been suggested that interactions of filopodia with a softer substrate may induce more branching [38]. The presence of collagen fibrils may make FN-COL matrices stiffer which could also contribute to the higher percentage of protrusions on FN matrix. We noted that the number of protrusions decreased over time on FN matrix while the number of branches increased. This raises the possibility that protrusions and branches are correlated and some of the protrusions may develop into branches.

It is well-established that adhesive cues in the ECM promote cytoskeletal rearrangements that are necessary for neurite outgrowth and are especially important for growth cone morphologies [35]. Neurite-ECM interactions induce actin filament formation and actin-myosin contractility. Differences in actin-mediated cell signals form the basis for changes in growth cone morphology between filopodial and slender [13,16] suggesting that the presence of collagen may cause retraction or prevent extension of protrusions. Overall, our results show that a fibrillar FN microenvironment provides permissive guidance cues for extension of neurites with enhanced production of actin-based cell processes. The deposition of collagen molecules may block some of the interactions that govern these processes. Our results provide new information about neuron responses to the major ECM components and how specific ECM proteins can modulate neuron behaviors required for nerve development and regeneration.

Supplementary Material

Refer to Web version on PubMed Central for supplementary material.

Acknowledgements

The authors thank members of Prof. Lynn Enquist's lab, Andrew Esteves and Shree Tanneti, for advice on rat embryo dissections and culturing neurons. We are grateful to Dr. Gary Laevsky, Director of Molecular Biology Confocal Microscopy Core Facility, a Nikon Center of Excellence, for his assistance with imaging, and Saw Kyin and Henry Shwe from Molecular Biology Proteomics and Mass Spectrometry Core facility for performing the mass spectrometric analyses. The authors also thank members of Schwarzbauer lab for thoughtful scientific discussions.

Funding

This work was supported by the Sud Cook '39 Fund for the Prevention of Addiction to Alcohol and other Mind-altering Drugs and by a grant from the National Institutes of Health NIAMS R01AR073236.

Availability of data and material

Materials are available upon request.

References

1. Hynes RO, Naba A (2012) Overview of the matrisome--an inventory of extracellular matrix constituents and functions. Cold Spring Harb Perspect Biol 4 (1):a004903. doi:10.1101/cshperspect.a004903 [PubMed: 21937732]
2. Muncie JM, Weaver VM (2018) The physical and biochemical properties of the extracellular matrix regulate cell fate. Curr Top Dev Biol 130:1–37. doi:10.1016/bs.ctdb.2018.02.002 [PubMed: 29853174]
3. Singh P, Carraher C, Schwarzbauer JE (2010) Assembly of fibronectin extracellular matrix. Annu Rev Cell Dev Biol 26:397–419. doi:10.1146/annurev-cellbio-100109-104020 [PubMed: 20690820]
4. Shechter R, Schwartz M (2013) Cns sterile injury: Just another wound healing? Trends Mol Med 19 (3):135–143. doi:10.1016/j.molmed.2012.11.007 [PubMed: 23279948]
5. Koopmans G, Hasse B, Sinis N (2009) Chapter 19: The role of collagen in peripheral nerve repair. Int Rev Neurobiol 87:363–379. doi:10.1016/S0074-7742(09)87019-0 [PubMed: 19682648]
6. Carvalho CR, Oliveira JM, Reis RL (2019) Modern trends for peripheral nerve repair and regeneration: Beyond the hollow nerve guidance conduit. Front Bioeng Biotechnol 7:337. doi:10.3389/fbioe.2019.00337 [PubMed: 31824934]
7. Grinsell D, Keating CP (2014) Peripheral nerve reconstruction after injury: A review of clinical and experimental therapies. Biomed Res Int 2014:698256. doi:10.1155/2014/698256 [PubMed: 25276813]
8. Gardiner NJ (2011) Integrins and the extracellular matrix: Key mediators of development and regeneration of the sensory nervous system. Dev Neurobiol 71 (11):1054–1072. doi:10.1002/dneu.20950 [PubMed: 21761574]
9. Flynn KC (2013) The cytoskeleton and neurite initiation. Bioarchitecture 3 (4):86–109. doi:10.4161/bioa.26259 [PubMed: 24002528]
10. Kalil K, Dent EW (2014) Branch management: Mechanisms of axon branching in the developing vertebrate cns. Nat Rev Neurosci 15 (1):7–18. doi:10.1038/nrn3650 [PubMed: 24356070]
11. Harris GM, Madigan NN, Lancaster KZ, Enquist LW, Windebank AJ, Schwartz J, Schwarzbauer JE (2017) Nerve guidance by a decellularized fibroblast extracellular matrix. Matrix Biol 60–61:176–189. doi:10.1016/j.matbio.2016.08.011
12. Singh S, Bandini SB, Donnelly PE, Schwartz J, Schwarzbauer JE (2014) A cell-assembled, spatially aligned extracellular matrix to promote directed tissue development. J Mater Chem B 2 (11):1449–1453. doi:10.1039/C3TB21864C [PubMed: 24707354]

13. Omotade OF, Pollitt SL, Zheng JQ (2017) Actin-based growth cone motility and guidance. Mol Cell Neurosci 84:4–10. doi:10.1016/j.mcn.2017.03.001 [PubMed: 28268126]
14. Short CA, Suarez-Zayas EA, Gomez TM (2016) Cell adhesion and invasion mechanisms that guide developing axons. Curr Opin Neurobiol 39:77–85. doi:10.1016/j.conb.2016.04.012 [PubMed: 27135389]
15. Wehner D, Tsarouchas TM, Michael A, Haase C, Weidinger G, Reimer MM, Becker T, Becker CG (2017) Wnt signaling controls pro-regenerative collagen xii in functional spinal cord regeneration in zebrafish. Nat Commun 8 (1):126. doi:10.1038/s41467-017-00143-0 [PubMed: 28743881]
16. Gomez TM, Letourneau PC (2014) Actin dynamics in growth cone motility and navigation. J Neurochem 129 (2):221–234. doi:10.1111/jnc.12506 [PubMed: 24164353]
17. Mao Y, Schwarzbauer JE (2005) Stimulatory effects of a three-dimensional microenvironment on cell-mediated fibronectin fibrillogenesis. J Cell Sci 118 (Pt 19):4427–4436. doi:10.1242/jcs.02566 [PubMed: 16159961]
18. Engler AJ, Chan M, Boettiger D, Schwarzbauer JE (2009) A novel mode of cell detachment from fibrillar fibronectin matrix under shear. J Cell Sci 122 (Pt 10):1647–1653. doi:10.1242/jcs.040824 [PubMed: 19401337]
19. Cukierman E, Pankov R, Yamada KM (2002) Cell interactions with three-dimensional matrices. Curr Opin Cell Biol 14 (5):633–639. doi:10.1016/s0955-0674(02)00364-2 [PubMed: 12231360]
20. To WS, Midwood KS (2011) Plasma and cellular fibronectin: Distinct and independent functions during tissue repair. Fibrogenesis Tissue Repair 4:21. doi:10.1186/1755-1536-4-21 [PubMed: 21923916]
21. Zareen N, Greene LA (2009) Protocol for culturing sympathetic neurons from rat superior cervical ganglia (scg). J Vis Exp (23). doi:10.3791/988
22. Harris GM, Raitman I, Schwarzbauer JE (2018) Cell-derived decellularized extracellular matrices. Methods Cell Biol 143:97–114. doi:10.1016/bs.mcb.2017.08.007 [PubMed: 29310794]
23. Raitman I, Huang ML, Williams SA, Friedman B, Godula K, Schwarzbauer JE (2018) Heparin-fibronectin interactions in the development of extracellular matrix insolubility. Matrix Biol 67:107–122. doi:10.1016/j.matbio.2017.11.012 [PubMed: 29223498]
24. Saunders JT, Schwarzbauer JE (2019) Fibronectin matrix as a scaffold for procollagen proteinase binding and collagen processing. Mol Biol Cell 30 (17):2218–2226. doi:10.1091/mbc.E19-03-0140 [PubMed: 31242089]
25. Tanaka A, Fujii Y, Kasai N, Okajima T, Nakashima H (2018) Regulation of neuritogenesis in hippocampal neurons using stiffness of extracellular microenvironment. PLoS One 13 (2):e0191928. doi:10.1371/journal.pone.0191928 [PubMed: 29408940]
26. Padayatty SJ, Levine M (2016) Vitamin c: The known and the unknown and goldilocks. Oral Dis 22 (6):463–493. doi:10.1111/odi.12446 [PubMed: 26808119]
27. Ren Y, Suter DM (2016) Increase in growth cone size correlates with decrease in neurite growth rate. Neural Plast 2016:3497901. doi:10.1155/2016/3497901 [PubMed: 27274874]
28. Jang KJ, Kim MS, Feltrin D, Jeon NL, Suh KY, Pertz O (2010) Two distinct filopodia populations at the growth cone allow to sense nanotopographical extracellular matrix cues to guide neurite outgrowth. PLoS One 5 (12):e15966. doi:10.1371/journal.pone.0015966 [PubMed: 21209862]
29. Igarashi M (2019) Molecular basis of the functions of the mammalian neuronal growth cone revealed using new methods. Proc Jpn Acad Ser B Phys Biol Sci 95 (7):358–377. doi:10.2183/pjab.95.026
30. Sakai T, Johnson KJ, Murozono M, Sakai K, Magnuson MA, Wieloch T, Cronberg T, Isshiki A, Erickson HP, Fassler R (2001) Plasma fibronectin supports neuronal survival and reduces brain injury following transient focal cerebral ischemia but is not essential for skin-wound healing and hemostasis. Nat Med 7 (3):324–330. doi:10.1038/85471 [PubMed: 11231631]
31. Grimpe B, Silver J (2002) The extracellular matrix in axon regeneration. Prog Brain Res 137:333–349. doi:10.1016/s0079-6123(02)37025-0 [PubMed: 12440376]
32. Shen Y (2014) Traffic lights for axon growth: Proteoglycans and their neuronal receptors. Neural Regen Res 9 (4):356–361. doi:10.4103/1673-5374.128236 [PubMed: 25206823]
33. Huebner EA, Strittmatter SM (2009) Axon regeneration in the peripheral and central nervous systems. Results Probl Cell Differ 48:339–351. doi:10.1007/400_2009_19 [PubMed: 19582408]

34. Tran AP, Warren PM, Silver J (2018) The biology of regeneration failure and success after spinal cord injury. Physiol Rev 98 (2):881–917. doi:10.1152/physrev.00017.2017 [PubMed: 29513146]

35. Dent EW, Gupton SL, Gertler FB (2011) The growth cone cytoskeleton in axon outgrowth and guidance. Cold Spring Harb Perspect Biol 3 (3). doi:10.1101/cshperspect.a001800

36. Lewis TL Jr., Courchet J, Polleux F (2013) Cell biology in neuroscience: Cellular and molecular mechanisms underlying axon formation, growth, and branching. J Cell Biol 202 (6):837–848. doi:10.1083/jcb.201305098 [PubMed: 24043699]

37. Gallo G (2011) The cytoskeletal and signaling mechanisms of axon collateral branching. Dev Neurobiol 71 (3):201–220. doi:10.1002/dneu.20852 [PubMed: 21308993]

38. Flanagan LA, Ju YE, Marg B, Osterfield M, Janmey PA (2002) Neurite branching on deformable substrates. Neuroreport 13 (18):2411–2415. doi:10.1097/00001756-200212200-00007 [PubMed: 12499839]

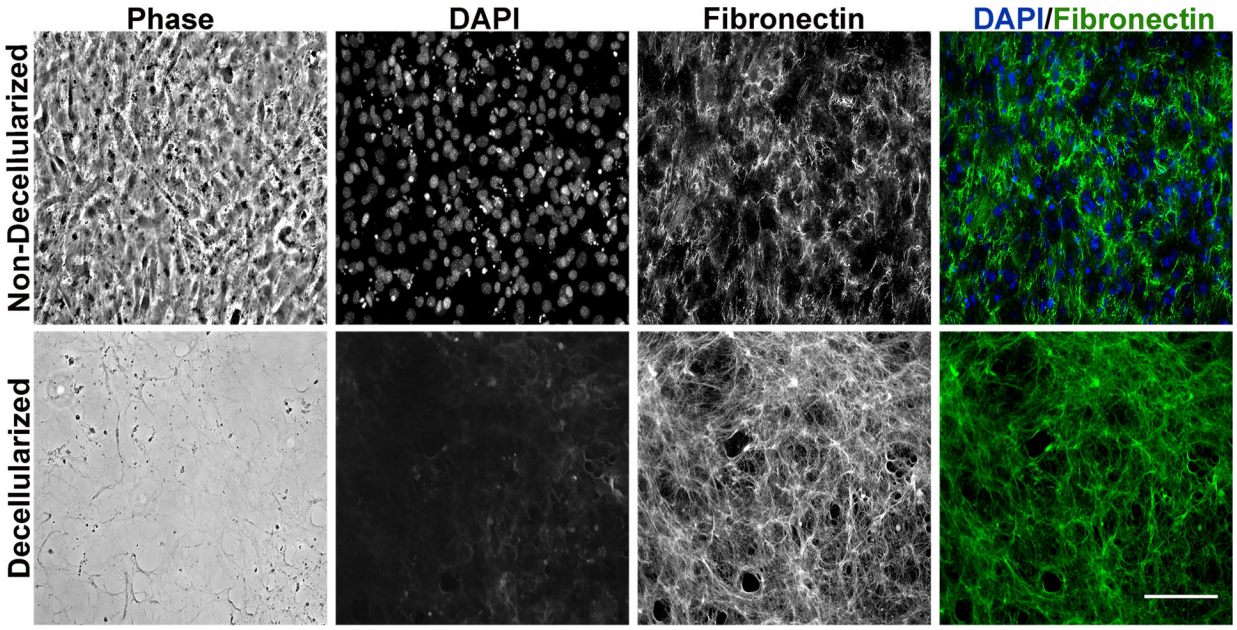

Fig. 1.

Three dimensional decellularized fibrillar fibronectin matrix. Confluent NIH 3T3 fibroblast cultures were fixed and stained (top) or were decellularized and the matrix was then fixed and stained (bottom). Non-decellularized and decellularized matrices were stained with R184 rabbit anti-FN antiserum followed by goat anti-rabbit IgG and DAPI for cells. Phase images show cell density and matrix fibrils without cells. Scale bar = 100 μm.

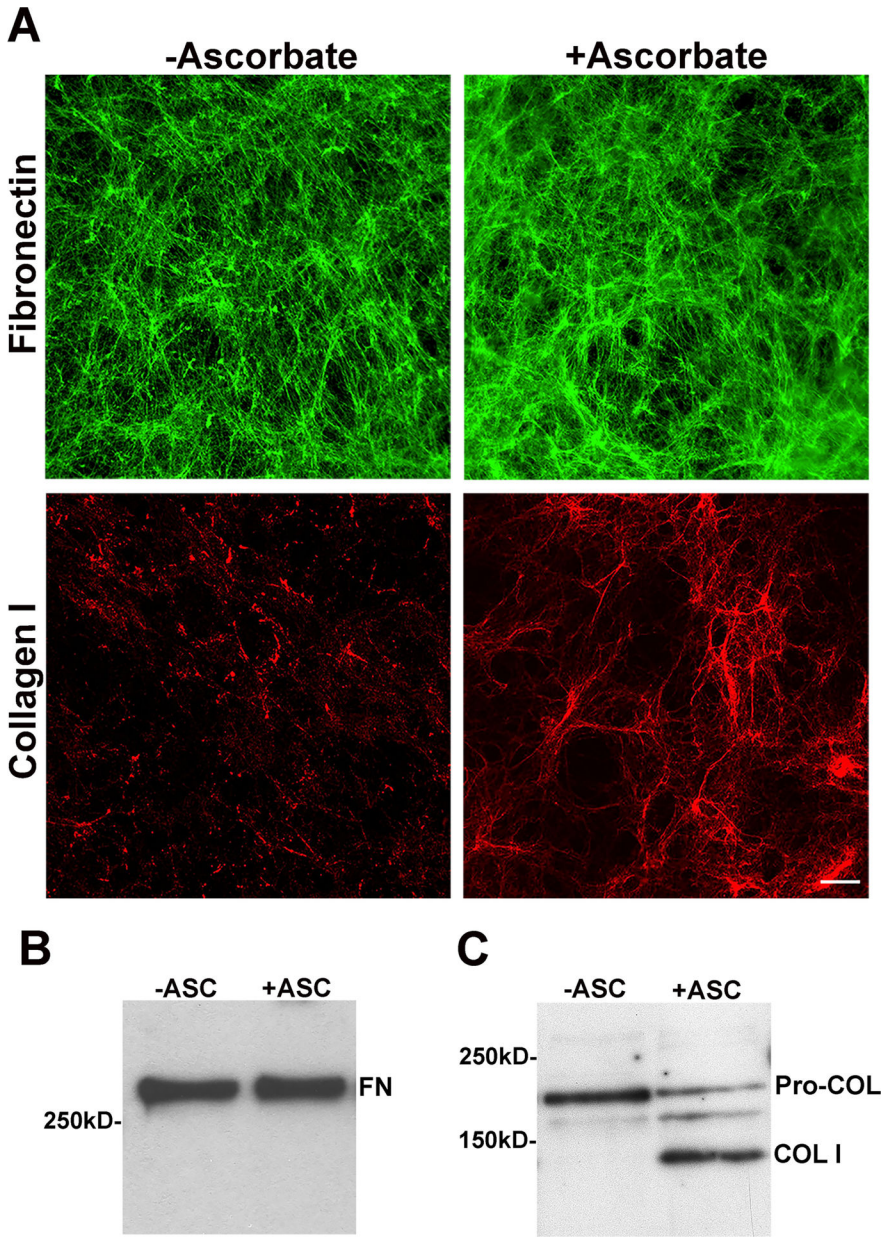

Fig. 2.

Characterization of decellularized fibrillar matrices. (A) Decellularized matrices prepared from cultures grown with or without ascorbate were immunostained with R184 antiserum (fibronectin, top) or with polyclonal anti-COL I antibody (Collagen I, bottom). Scale bar = 100 μm. Decellularized matrices -ascorbate (-ASC) or +ascorbate (+ASC) were solubilized in SDS buffer, resolved by SDS-PAGE (6% polyacrylamide gel) and immunoblotted with R184 antiserum (B, FN) and anti-COL I antibodies (C). Locations of procollagen I (Pro-COL) and processed collagen I (COL I) bands are indicated. Molecular weight markers are indicated on the left of each blot.

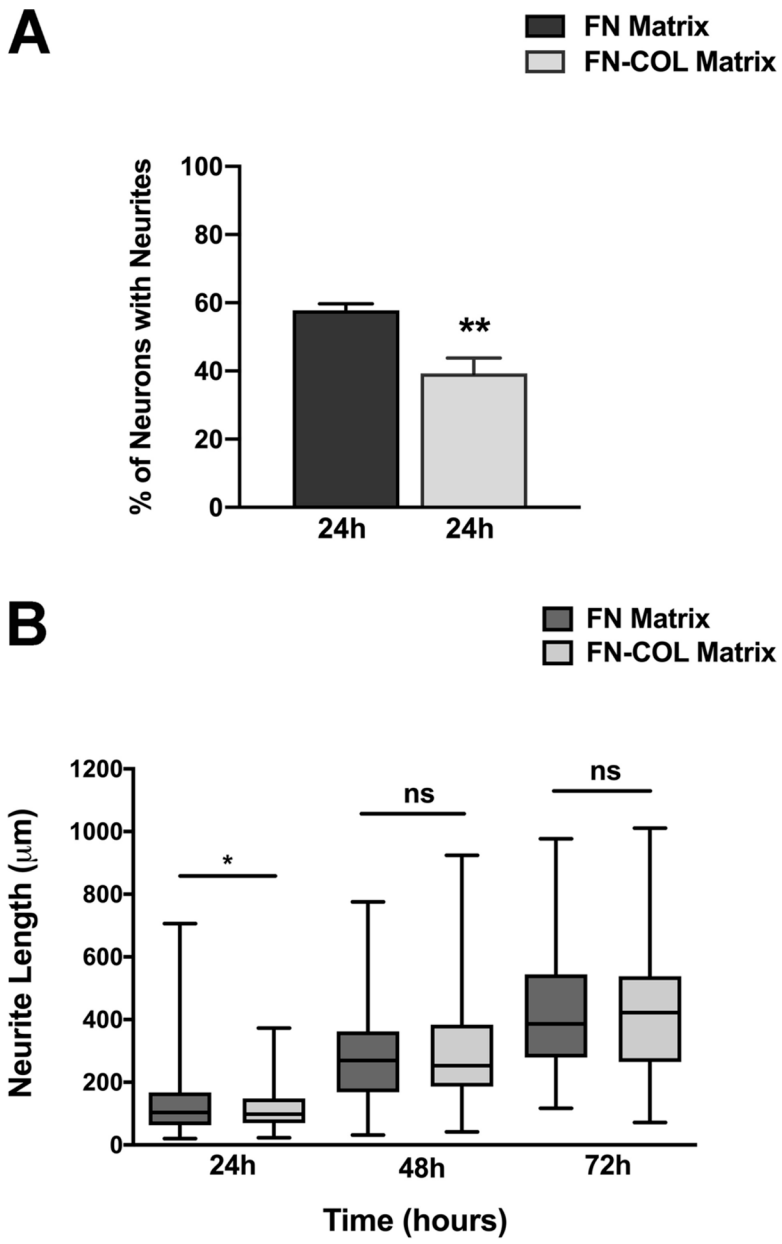

Fig. 3.

Percentage of neurons extending neurites and neurite length on decellularized FN and FN-COL matrices. (A) Percentage of neurons with neurites was determined on FN and FN-COL matrices after 24h. Bar is the average from three independent experiments, expressed as mean ± SEM. (B) Neurite lengths were measured at 24h, 48h and 72h. Box-whisker plots (box representing 25^{th} and 75^{th} percentile, middle line indicating the median, and whiskers representing the min and max values) calculated from three independent experiments. Two-tailed unpaired t-test with Welch correction was used to compare % of neurons with neurites and neurite lengths between FN and FN-COL matrices at each time point. ** $P \leq 0.01$; * $P \leq 0.05$; ns= not significant, $P > 0.05$. For total number (n) of neurites measured see Table 1.

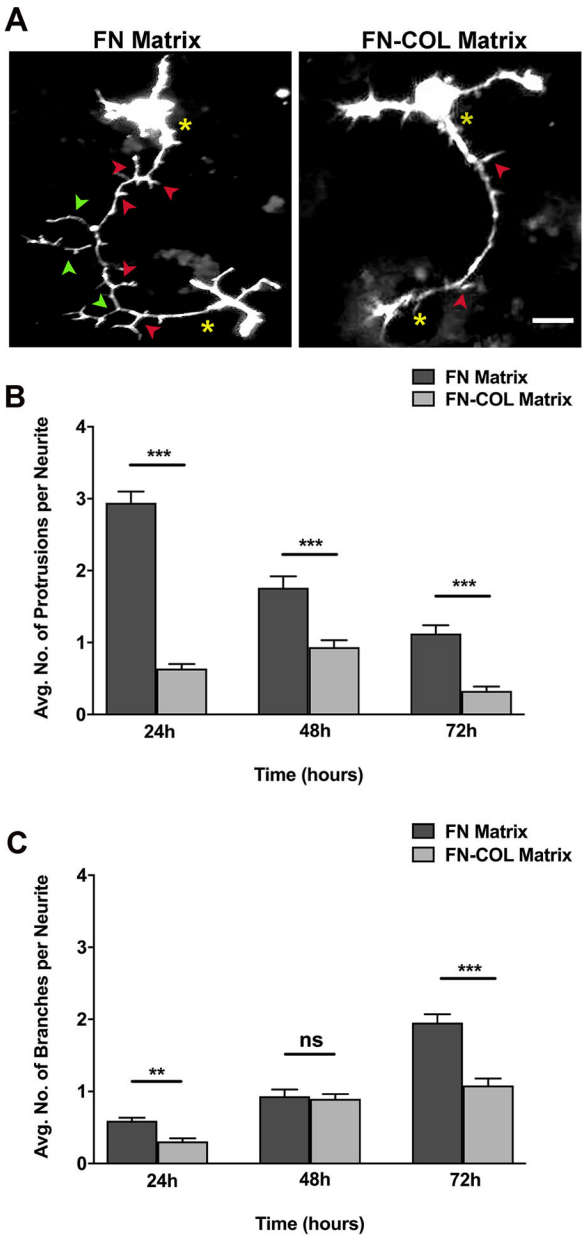

Fig. 4.

Protrusions and branches extended from neurites on decellularized FN and FN-COL matrices. (A) Examples of SCG neurons are shown grown on FN matrix or FN-COL matrix for 24h and stained with rhodamine-phalloidin to visualize actin filaments. Representative examples of protrusions (red arrowheads) and branches (green arrowheads) extending from neurite shafts (start and end marked with yellow star) are indicated. Scale bar = 10 μm. (B, C) Protrusions and branches were scored and the average number per neurite was calculated for each time point across three independent experiments. Averages per neurite on FN matrix (dark gray) and on FN-COL matrix (light gray) are plotted. (B) Protrusions per neurite, (C) branches per neurite. One-way ANOVA with Bonferroni post-test was used to

compare average number of protrusions and branches in both matrices. *** $P \leq 0.001$, ** $P \leq 0.01$, ns = not significant, $P > 0.05$. Measurements were expressed as mean ± SEM.

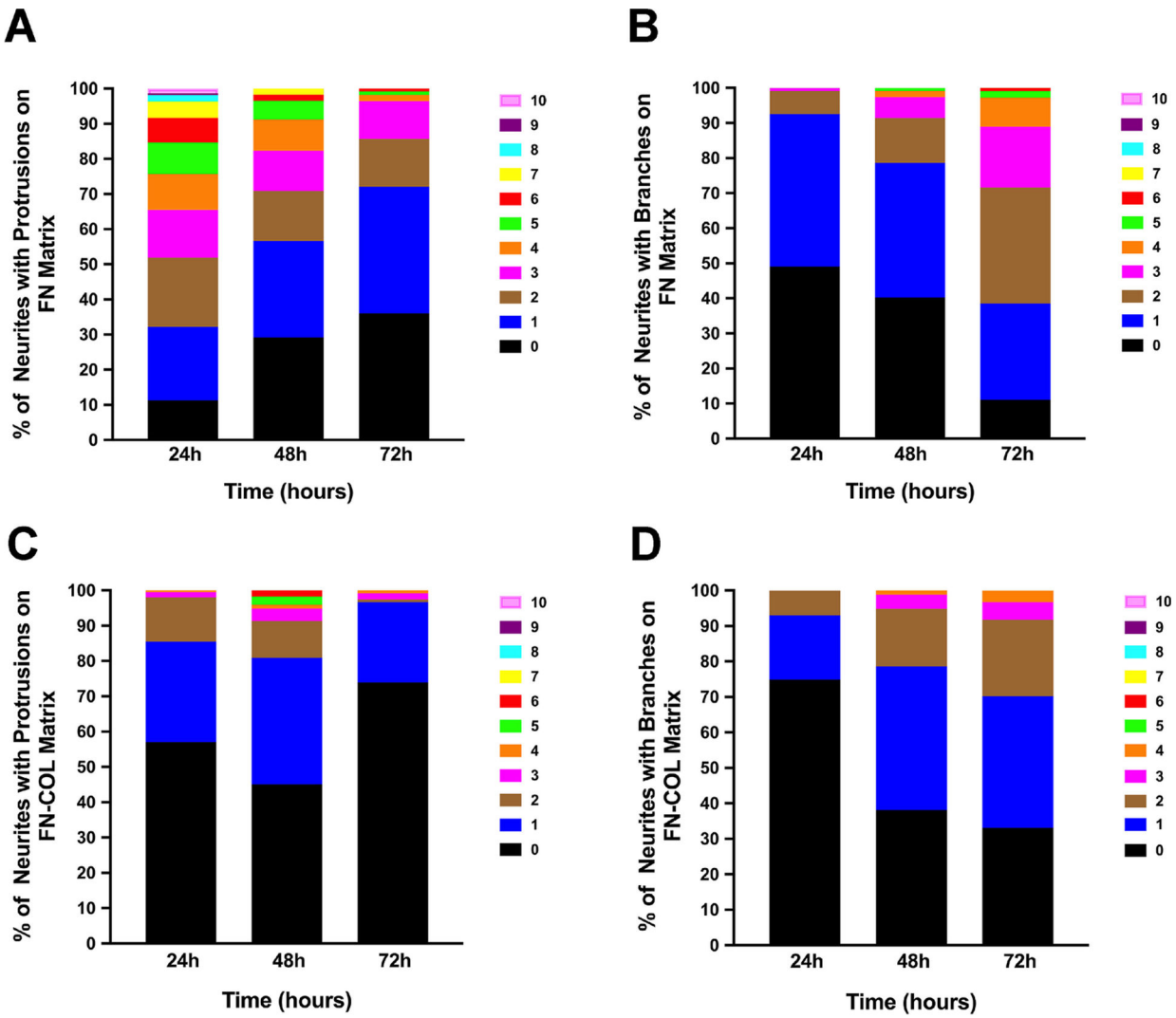

Fig. 5.

Percentage of neurites containing different numbers of protrusions and branches on decellularized FN and FN-COL matrices. The percentages of neurites with protrusions (A, C) and branches (B, D) on FN matrix (A, B) or FN-COL matrix (C, D) were calculated for each time point across three independent experiments. Legend to the right of each graph identifies color-coding. Number (n) of neurites measured is given in Table 1.

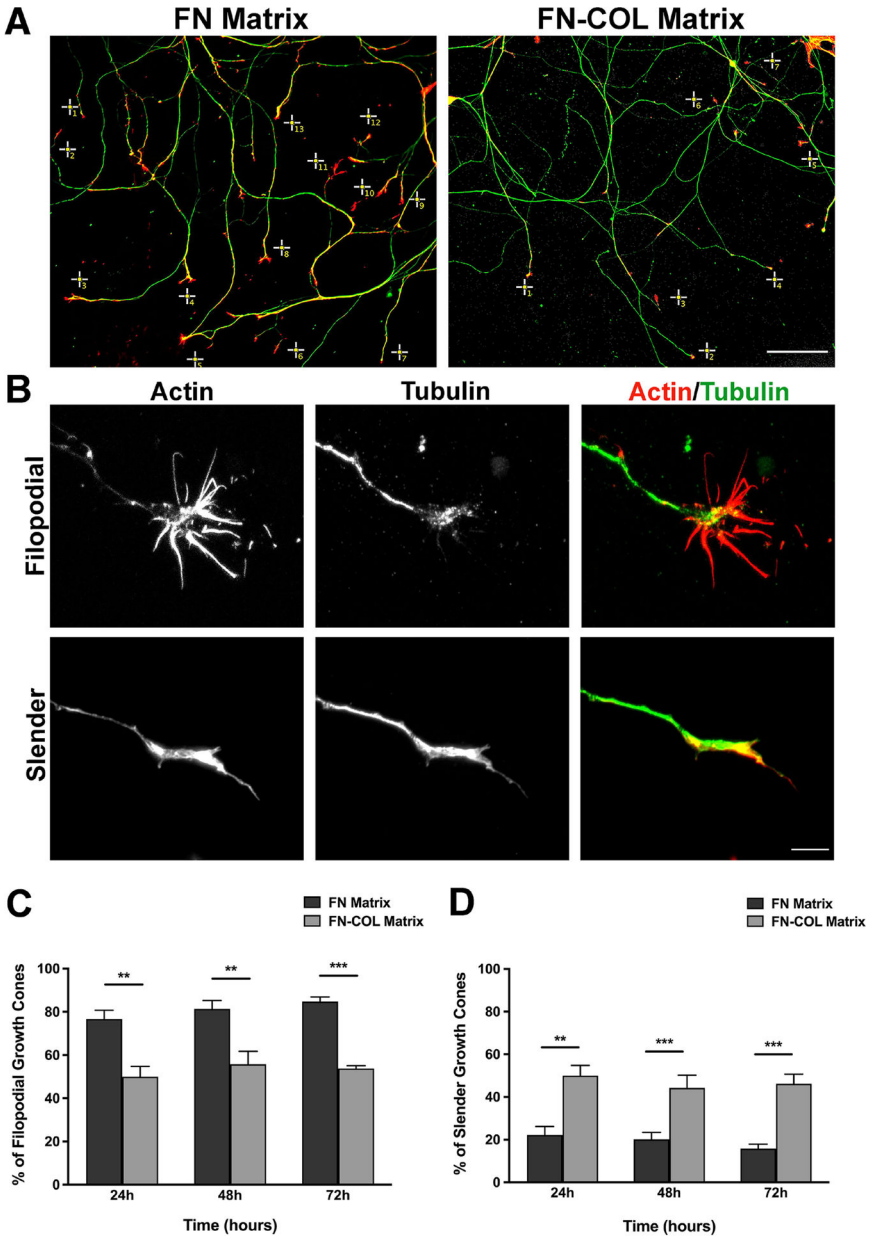

Fig. 6.

Growth cone morphologies on decellularized FN and FN-COL matrices. (A) Merged images of the neurites with growth cones are shown on FN and FN-COL matrix stained with anti-α-tubulin antibody followed by fluorescein-goat anti-mouse IgG (green) and with rhodamine-phalloidin (red). Scale bar = 100 μm. (B) Two different growth cone morphologies predominate on decellularized matrices. Confocal images of growth cones stained as in (A) show the fan-shaped filopodial morphology with actin-filled projections (top). Slender growth cones have overlapping actin and tubulin staining (bottom). Scale bar = 20 μm. The percent of filopodial (C) and slender (D) growth cone morphologies were compared between the matrices (FN, dark gray; FN-COL, light gray). SCG growth cones stained for actin filaments were scored in three independent experiments. One-way ANOVA

with Bonferroni post-test was used to compare % of filopodial and slender growth cones on the two matrices at each time point. *** $P \leq 0.001$, ** $P \leq 0.01$. Measurements were expressed as mean ± SEM. For total number (n) of growth cones measured see Table 3.

Table 1:

Analysis of neurite lengths on different decellularized matrices

	FN Matrix		FN-COL Matrix	
Time	**No. of Neurites[a]**	**Avg. Length (μm)[b]**	**No. of Neurites[a]**	**Avg. Length (μm)[b]**
24h	212	133.51 ± 07.12	199	110.18 ± 04.67
48h	114	277.78 ± 12.97	170	291.99 ± 11.65
72h	108	425.94 ± 17.25	115	413.73 ± 18.14

[a]Total number of neurites measured.

[b]Average of three independent experiments ± SEM.

Table 2:

Numbers of protrusions and branches per neurite on decellularized matrices

	FN Matrix		FN-COL Matrix	
Time	**Avg. No. of Protrusions[a]**	**Avg. No. of Branches[a]**	**Avg. No. of Protrusions[a]**	**Avg. No. of Branches[a]**
24h	2.9 ± 0.2	0.6 ± 0.0	0.6 ± 0.1	0.3 ± 0.0
48h	1.8 ± 0.2	0.9 ± 0.1	0.9 ± 0.1	0.9 ± 0.1
72h	1.1 ± 0.1	2.0 ± 0.1	0.3 ± 0.1	1.1 ± 0.1

[a]Average of three independent experiments ± SEM. Total numbers of neurites are the same as Table 1.

Table 3:

Growth cone morphologies on FN versus FN-COL matrices

	FN Matrix			FN-COL Matrix		
Time	**No. of Growth Cones**[a]	**% of Slender**[b]	**% of Filopodial**[b]	**No. of Growth Cones**[a]	**% of Slender**[b]	**% of Filopodial**[b]
24h	102	22.20 ± 04.01	76.68 ± 04.05	178	50.33 ± 04.77	49.97 ± 04.77
48h	139	20.13 ± 03.28	81.33 ± 03.91	115	44.24 ± 05.97	55.67 ± 05.97
72h	125	15.79 ± 02.11	84.75 ± 02.17	127	46.20 ± 04.50	53.80 ± 01.26

[a]Total number of growth cones

[b]Average of three independent experiments ± SEM.